npj | climate and atmospheric science

www.nature.com/npjclimatsci

ARTICLE OPEN

Check for updates

Mechanism-based structure-activity relationship investigation on hydrolysis kinetics of atmospheric organic nitrates

Qiaojing Zhao[1], Hong-Bin Xie[1]✉, Fangfang Ma[1], Wei Nie[2], Chao Yan[2], Dandan Huang[3], Jonas Elm[4] and Jingwen Chen[1]

Organic nitrates are key components of atmospheric organic aerosols. Hydrolysis is one of their main transformation pathways, affecting atmospheric nitrogen cycle and the properties of organic aerosols. Studying hydrolysis using experiments is hindered by limited authentic chemical standards. To advance our understanding on the hydrolysis of organic nitrates, we apply quantum chemistry methods here to establish a structure-activity relationship of the mechanisms and kinetics by selecting eight organic nitrates as model compounds. The results indicate that an acid-catalyzed mechanism is dominant for the most considered organic nitrates at pH corresponding to ambient organic aerosol (pH < 5). More importantly, a hydrolysis pathway driven by the shift of hydrogen or methyl cation is unveiled. Based on the revealed mechanisms, quaternary C at the α-site, tertiary/quaternary C at the β-site, and –C=C at the β/γ-site of the $-ONO_2$ group are determined to be the key structural factors for the fast hydrolysis kinetics. An important feature for the hydrolysis of organic nitrates with such structural factors is proceeding via a carbocation intermediate. The formed carbocation could further mediate the organic aerosol chemistry, affecting the composition and properties of organic aerosols. This study provides a basis to further develop predictive models for hydrolysis kinetics of organic nitrates.

npj Climate and Atmospheric Science (2023)6:192 ; https://doi.org/10.1038/s41612-023-00517-w

INTRODUCTION

Atmospheric organic aerosol are known to have an effect on the global climate and human health[1,2]. Throughout the atmospheric lifecycle of organic aerosol, complicated particle-phase reactions can occur[3–10], dramatically altering the composition and properties of the organic aerosol[11–13]. Therefore, studying the particle-phase chemistry is essential for understanding the environmental impact of organic aerosols. In recent years, particle-phase chemistry of organic compounds has received increasing attention[3–13]. However, the studies are still very scarce compared to the extensively studied gas-phase chemistry. Thus, more efforts should be undertaken to establish a comprehensive understanding of atmospheric particle-phase chemistry.

Organic nitrates are key components of organic aerosol, accounting for fractions ranging from 5 to 77% depending on the location[14–20]. Recently, the ambient detection of particulate organic nitrates has been carried out. For example, Lee et al. detected 88 highly functionalized organic nitrates resulting from oxidation of biogenic hydrocarbons in rural Alabama, America. These organic nitrates demonstrate a high rate of loss[21]. Shi et al. identified 78 organic nitrates, most of which originate from anthropogenic hydrocarbons, in urban atmosphere of Beijing, China during 2016–2018[22]. Due to their high mass fraction, close relevance to atmospheric nitrogen cycle and ozone budget, and potential for high rates of loss[21,23–26], understanding the chemistry of organic nitrates becomes increasingly important. Hydrolysis has been identified as a critical transformation pathway for particulate organic nitrates[13,27–41]. Different from the direct photolysis or degradation via oxidation reactions, hydrolysis transforms the $-ONO_2$ functional group to HNO_3, thereby acting as a permanent sink of NO*x*[25,30,41,42]. More importantly, it was found that implementing the hydrolysis pathway of even a single isoprene hydroxyl-nitrate in an atmospheric model could substantially reduce the simulated concentrations of NO and O_3[31]. Therefore, it is important to investigate the hydrolysis mechanism and kinetics of various atmospheric organic nitrates.

Currently, the authentic chemical standard for organic nitrates is lacking, which makes it necessary for experimental studies on hydrolysis kinetics to synthesize target organic nitrates first. To the best of our knowledge, experimental hydrolysis kinetic data is only available for about twenty organic nitrates, and most experimental studies were conducted under different conditions such as different pH values and buffer systems[32,33,35,36]. Two reaction pathways, namely the bimolecular substitution (S_N2) and the unimolecular substitution (S_N1) pathways, have been proposed for the hydrolysis of organic nitrates[35,36,39]. Nonetheless, there is a lack of detailed mechanistic insight into the effect of structural factors on hydrolysis kinetics, except for the fact that organic nitrates with quaternary C at the α-site of the $-ONO_2$ group exhibit fast reaction kinetics. The insufficiency of kinetic data and a lack of deep mechanistic insight render it impossible to generalize the results to other atmospherically relevant organic nitrates. To advance the hydrolysis chemistry of organic nitrates and overcome the difficulties in experimental studies, an alternative strategy should be proposed to perform a mechanism-based structure-activity relationship study on hydrolysis kinetics.

In this study, we utilized a quantum chemical method to establish the structure-activity relationship for the hydrolysis kinetics of organic nitrates by studying the reaction mechanism and kinetics of eight organic nitrates including primary, secondary and tertiary organic nitrates. Specifically, three primary organic nitrates (ethyl nitrate (ETN), isobutyl nitrate (IBN), and [4-(2-hydroxypropan-2-yl)cyclohexen-1-yl]methyl nitrate (BpON), two secondary organic nitrates (isopropyl nitrate (IPN) and

[1]Key Laboratory of Industrial Ecology and Environmental Engineering (Ministry of Education), School of Environmental Science and Technology, Dalian University of Technology, Dalian 116024, China. [2]Joint International Research Laboratory of Atmospheric and Earth System Sciences, School of Atmospheric Sciences, Nanjing University, Nanjing 210023, China. [3]State Environmental Protection Key Laboratory of Formation and Prevention of Urban Air Pollution Complex, Shanghai Academy of Environmental Sciences, Shanghai, China. [4]Department of Chemistry, iClimate, Aarhus University, Langelandsgade 140, DK-8000 Aarhus C, Denmark. ✉email: hbxie@dlut.edu.cn

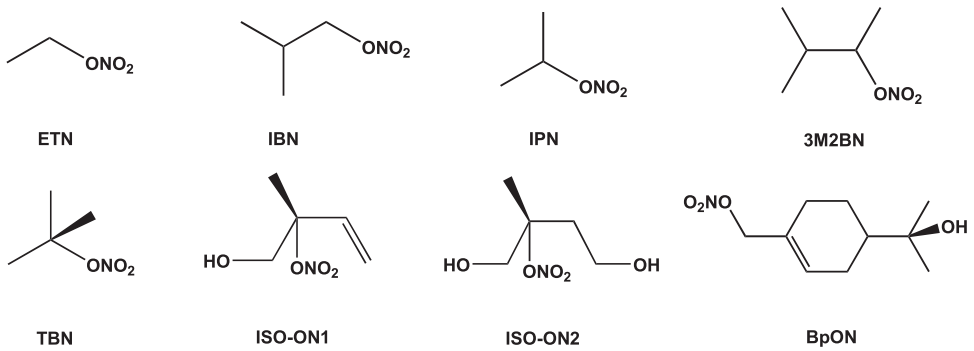

Fig. 1 Molecular structures of the selected eight organic nitrates.

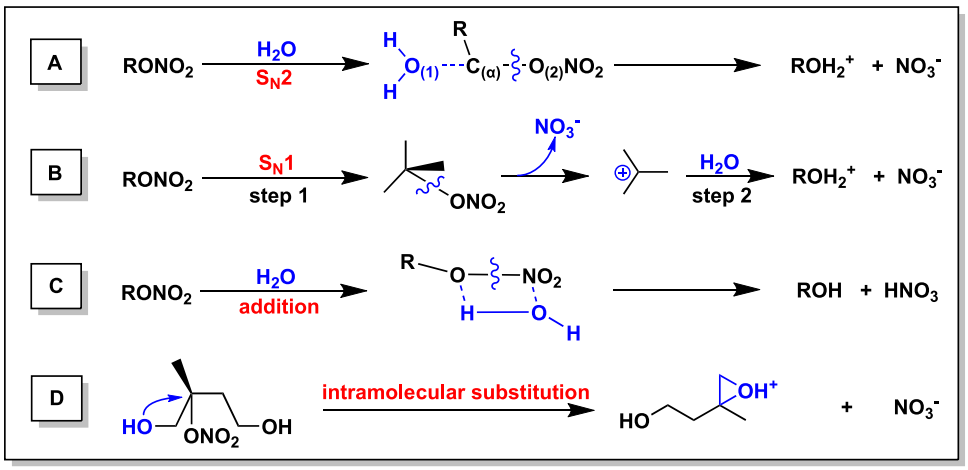

Fig. 2 Schematic diagram of neutral hydrolysis pathways. A–D represent S_N2, S_N1, H_2O addition and intramolecular substitution reaction pathways.

3-methyl-2-butanyl nitrate (3M2BN)), and three tertiary organic nitrates (*tert*-butyl nitrate (TBN), (2-hydroxy-2-methylbut-3-enyl) nitrate (ISO-ON1) and (1,4-dihydroxy-2-methylbutyl) nitrate (ISO-ON2)) (Fig. 1) were studied by comprehensively considering neutral, basic, and acid-catalyzed hydrolysis reactions. All selected eight organic nitrates have been identified in the atmosphere[21,43–46]. Another main consideration for selecting these organic nitrates as model compounds is structural diversity of the α and β-site of the $-ONO_2$ group. The revealed mechanism-based structure-activity relationship can be employed to judge the possible hydrolysis chemistry of target organic nitrates and embedded into atmospheric models to roughly estimate the kinetics of other atmospheric organic nitrates.

RESULTS AND DISCUSSION

Three types of hydrolysis mechanism i.e., neutral, basic, and acid-catalyzed hydrolysis were investigated for all eight organic nitrates. The most favorable pathways determined for each mechanism considered are presented in Figs. 3, 5 and 7, with remaining pathways in Supplementary Figs. 1–24.

Neutral hydrolysis mechanism

Within the neutral hydrolysis mechanism, four kinds of reaction pathways consisting of S_N2, S_N1, intramolecular substitution and H_2O addition were identified (Fig. 2). The S_N2 pathway is a one-step process via H_2O attacking on the α-C-atom (C_α) of the $-ONO_2$ group, leading to the formation of a protonated alcohol (ROH_2^+) and nitrate ion (NO_3^-). While the S_N1 reaction pathway proceeds via two steps, starting with the rupture of the $C_\alpha-O_{(2)}$ bond connecting the C_α and the $-ONO_2$ group to generate a carbocation and NO_3^-, followed by the combination of the carbocation with H_2O to produce ROH_2^+. However, we cannot successfully locate all transition states (TSs) of the S_N1 pathway for eight organic nitrates apart from the second step of ISO-ON1 although lots of attempts were performed. Since the first step is endothermic and the second step is exothermic for the S_N1 pathway, the relaxed scan method was only employed to investigate the free-energy barrier for the first step of the S_N1 pathway (see Supplementary Methods and Supplementary Figs. 25–27). The intramolecular substitution reaction pathway is driven by the $-OH$ group at the C_β attacking the C_α of the $-ONO_2$ group. For the H_2O addition pathway, the $-H$ and $-OH$ of H_2O are added to $O_{(2)}$ and N sites of the $-ONO_2$ group, respectively, leading to the formation of a neutral alcohol (ROH) and nitric acid (HNO_3).

Amongst the studied eight compounds, the primary and secondary organic nitrates hydrolyze via S_N2, S_N1 and H_2O addition reaction pathways and the tertiary ones via S_N1 and H_2O addition reaction pathways. Moreover, the ISO-ON2 also can hydrolyze via the intramolecular substitution pathway. By comparing the free-energy barriers of all possible reaction pathways for each organic nitrate, it was found that the S_N2 pathway is dominant for ETN, S_N1 pathway for BpON, TBN, ISO-ON1 and ISO-ON2, and the S_N2 and S_N1 pathways are competitive for IBN, IPN and 3M2BN. Figure 3 shows the dominant pathways and Supplementary Fig. 28 gives the calculated structures and key bond distances of the transition states involved in neutral hydrolysis of organic nitrates. We found that all the neutral reaction pathways have to at least overcome a free-energy barrier of 26.95 kcal mol^{-1}. Therefore, the contribution of the neutral mechanism to the hydrolysis of organic nitrates is negligible. It

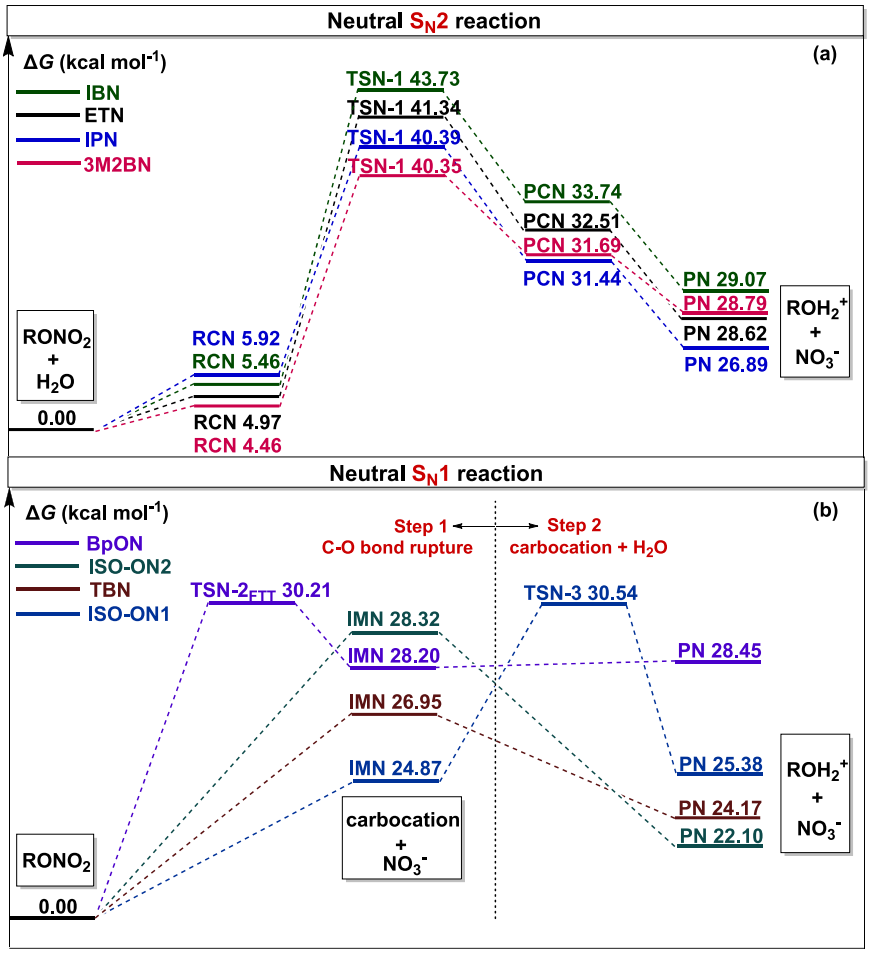

Fig. 3 Calculated schematic free-energy surfaces for the most favorable neutral hydrolysis pathway of studied organic nitrates ($RONO_2$) at the PCM_UFF/CBS-QB3//M06-2X/6-31+G(d,p) level. a Neutral S_N2 pathway. **b** Neutral S_N1 pathway. The free energies of $RONO_2 + H_2O$ and $RONO_2$ are set to zero (reference state). RCN, TSN-*m* (*m* = 1, 2, 3), PCN, IMN, and PN represent pre-reactive complexes, transition states, post-reactive complexes, intermediates, and products, respectively; where *m* denotes different transition states. $TSN\text{-}2_{FIT}$ denotes the fitted transition state using the relaxed scan method for the S_N1 pathway of BpON.

should be noted that previous study reported that there may be errors in the calculation of the entropy effect using the relaxed scan method and therefore the error for calculated free-energy barrier value for feasible S_N1 pathway could become greater[47]. Due to the very high free-energy barrier, the error in calculated free-energy barrier of S_N1 pathway should not change qualitative conclusion.

Basic hydrolysis mechanism

For the basic hydrolysis mechanism, four different pathways including two-step reaction initiated by the addition of the hydroxide ion (simply called OH^- addition in the whole text), S_N2, bimolecular elimination (E2) reaction and proton-abstraction pathway (illustrated in Fig. 4) were considered for all studied organic nitrates. The two-step pathway is initiated by OH^- addition on the N site to form an intermediate, followed by the concerted shift of the hydrogen cation (simply called H-shift in the whole text) and the $O_{(2)}$–N bond rupture to form a ROH and NO_3^-. It deserves mentioning that the formation of the intermediate proceeds via a pre-reactive complex. As shown in Supplementary Figs. 29 and 30, the key $O_{(3)}$–N bond distance varies greatly from the pre-reactive complex to the intermediates (from 2.90 Å to 1.50 Å). The S_N2 pathway is similar to that of neutral hydrolysis, with OH^- attacking the C_α to form a ROH and NO_3^-. The E2 pathway is the concerted one with OH^- abstracting a proton from the C_β and the C_α–$O_{(2)}$ bond rupturing to form an olefin, NO_3^- and H_2O. Alternatively, OH^- abstracts a proton from the C_α and the $O_{(2)}$–N bond rupture to form a ketone, NO_2^- and H_2O. The proton-abstraction pathway leads to the formation of carbanion and H_2O.

As can be seen in Fig. 5, the two-step reaction pathway initiated by OH^- addition is most favorable for all of the studied organic nitrates except the three tertiary ones. The first step is the rate-determining one since the second-step is barrier-less for the two-step hydrolysis pathway. Three exceptions are observed for the tertiary organic nitrates TBN, ISO-ON1, and ISO-ON2, which follow the E2 pathway to form the corresponding olefins, NO_3^- and H_2O. Therefore, the general trend is that the primary and secondary organic nitrates prefer to the two-step reaction pathway, while tertiary organic nitrates prefer to E2 pathway. Differing from the neutral hydrolysis, all the identified basic hydrolysis pathways are significantly exothermic and have a much lower free-energy barrier (15.36–18.18 kcal mol^{-1}). In addition, the difference in the free-energy barrier for the most favorable basic hydrolysis pathway of the eight organic nitrates is small (<3 kcal mol^{-1}), implying that structural factors have a slight effect on the basic hydrolysis mechanism.

Acid-catalyzed hydrolysis mechanism

Generally, the protonated process of the $-ONO_2$ group for organic nitrates is thermodynamically controlled. Therefore, in the

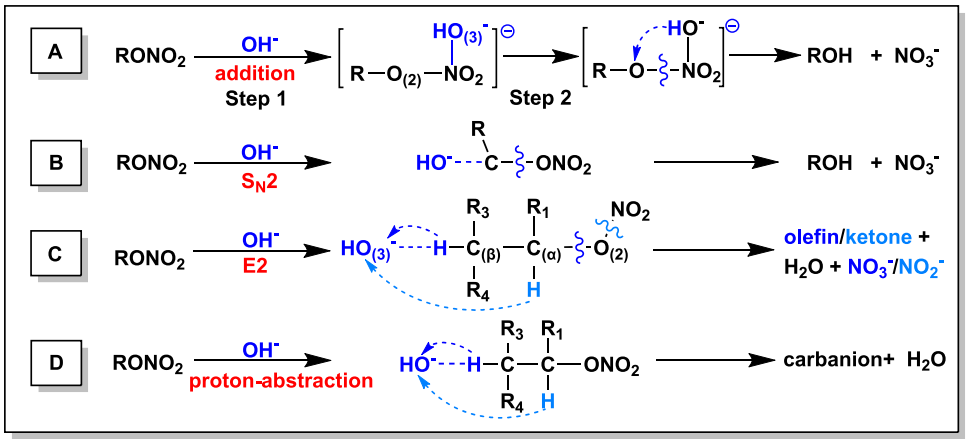

Fig. 4 Schematic diagram of basic hydrolysis pathways. A–D represent OH^- addition, S_N2, E2 and proton-abstraction pathways.

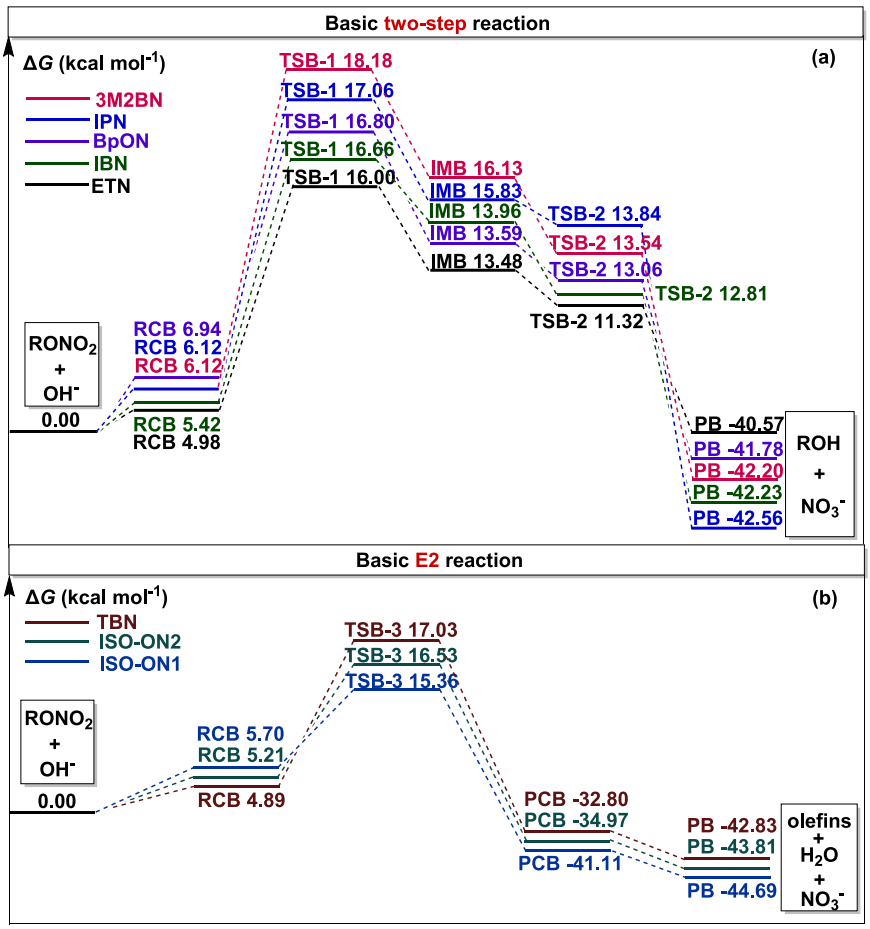

Fig. 5 Calculated schematic free-energy surfaces for the most favorable basic hydrolysis pathway of studied organic nitrates ($RONO_2$) at the PCM_UFF/CBS-QB3//M06-2X/6-31+G(d,p) level. a Basic two-step reaction. **b** Basic E2 reaction. The free energies of $RONO_2 + OH^-$ are set to zero (reference state). RCB, TSB-*m* (*m* = 1, 2, 3), PCB, IMB, and PB represent pre-reactive complexes, transition states, post-reactive complexes, intermediates, and products, respectively, where *m* denotes different transition states.

acid-catalyzed hydrolysis of organic nitrates, the R-ONO_2 and H_3O^+ were selected as the starting reactants for the free energy calculation and mechanism discussion starting from the protonated organic nitrates. We considered three types of acid-catalyzed hydrolysis pathways including S_N2, S_N1 and H-shift between the C_α and the C_β of the $-ONO_2H$ group for the selected organic nitrates (Fig. 6). The S_N2 pathway is similar to that of neutral and basic hydrolysis, with H_2O attacking the C_α of the $-ONO_2H$ group to form a ROH_2^+ and HNO_3. Similar to the neutral hydrolysis, the S_N1 reaction pathway proceeds in two steps via a carbocation to generate ROH_2^+ and HNO_3. The H-shift pathway has two outcomes: one is the reaction initiated by the C_α–$O_{(2)}$ bond rupture to form a carbocation and HNO_3, followed by the carbocation combining with H_2O to produce a ROH_2^+, while the other is a concerted reaction with the migration of the $-ONO_2H$ group, leading to an exchange of an H atom at the C_β with the

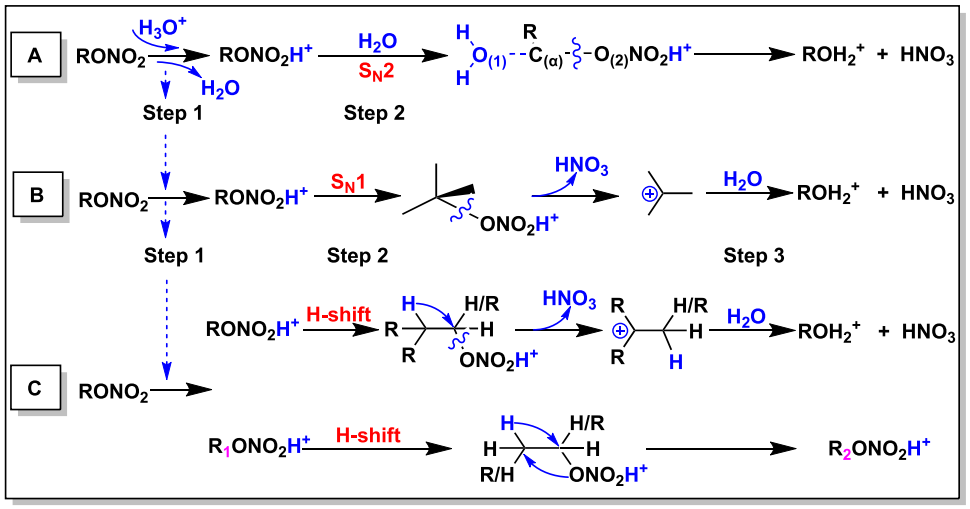

Fig. 6 Schematic diagram of acid-catalyzed hydrolysis pathways. A–C represent S_N2, S_N1, and H-shift reaction pathways.

$-ONO_2H$ group. It should be noted that not all three pathways were identified for each of the studied organic nitrates, and the available acid-catalyzed hydrolysis pathway is highly dependent on the specific structure of the organic nitrates. As shown in Supplementary Figs. 17–24, the S_N2 pathway was identified for the primary organic nitrates except BpON, the H-shift pathways for the primary and secondary organic nitrates (if there is an H-atom at the C_β) and the S_N1 pathway for all organic nitrates except primary organic nitrates ETN and IBN.

As shown in Fig. 7, the S_N2 pathway is most favorable for the primary organic nitrate ETN and the S_N1 or H-shift pathway is most favorable for the remaining organic nitrates. Here, we confirmed the H-shift-assisted hydrolysis pathway is feasible except the S_N2 and S_N1 pathways. The structures and key bond distances for the TSs of the rate-determining step for these pathways are presented in Supplementary Fig. 31. It deserves mentioning that the free-energy barrier in the first step of the S_N1 pathway for IPN was obtained by the relaxed scan method similar to the neutral case (Supplementary Figs. 32 and 33).

Almost all precursors that follow the S_N1 or H-shift pathway are either tertiary organic nitrates or primary and secondary organic nitrates with a tertiary C and –C=C at the β-site of the $-ONO_2H$ group except for the IPN with greater uncertainty. All favorable S_N1 or H-shift pathways proceed via two steps with the carbocation as the reaction intermediate. Interestingly, only two types of carbocations i.e., a tertiary one and a delocalized primary one (there is a double bond at α-site of the carbocation) were formed in regardless of S_N1 or H-shift reaction pathway. From an electronic structure perspective, the tertiary and delocalized carbocations should be much more stable than the simple primary and secondary carbocation[48–50]. Therefore, the formation of the stable carbocations should be the reason why these precursors follow the S_N1 or H-shift pathway.

Kinetics of organic nitrates hydrolysis

Based on the most favorable reaction pathway, we calculated the neutral (k'_N), basic (k'_B), acid-catalyzed (k'_A), and total (k_T) pseudo-first-order hydrolysis rate constants (Supplementary Table 1) for all eight organic nitrates. The logarithmic values of the calculated pseudo-first-order hydrolysis rate constants were then plotted against pH in Fig. 8, alongside available experimental data. We can see that the logarithmic values of k'_A are higher than those of the corresponding k'_N and k'_B for all considered organic nitrates except ETN and IBN under pH < 5, suggesting that acid-catalyzed hydrolysis is the dominant mechanism for most organic nitrates, given that the pH of atmospheric aerosol particles is typically below 5[6,51]. For the exception ETN and IBN, acid-catalyzed hydrolysis is dominant under pH < 3, with basic hydrolysis being the more dominant mechanism otherwise.

The logarithmic values of k_T for TBN, ISO-ON1, ISO-ON2, BpON, and 3M2BN are much higher than those of ETN, IBN, and IPN. A common feature for the organic nitrates with large k_T values is that they all follow either an S_N1 or H-shift reaction pathway that proceeds via a stable carbocation, highlighting the key role of stable carbocations in facilitating hydrolysis. Such role of carbocation is further supported by comparing the logarithmic values of k_T for two organic nitrates of the same type, one following the S_N2 pathway or the S_N1 pathway via a secondary carbocation and the other proceeding via a two-step reaction pathway initiated by H-shift with the stable tertiary carbocations as intermediates, e.g., ETN and IBN, or IPN and 3M2BN.

Comparing the calculated k_T values with the experimental ones, the deviation between them is about 0-2 orders of magnitude except for IPN and BpON at low pH values. As we mentioned in the *neutral hydrolysis mechanism* part, the possible errors in the calculation of the entropy effect using the relaxed scan method should be the reason for the larger deviation for IPN. In addition, by comparing energetic information for the most favorable pathways of BpON with that of other studied systems, it was found that the hydrolysis of BpON was slightly endothermic, which can make inverse reaction proceed fast. The reversible hydrolysis reaction of BpON was also suggested in the experimental study[35]. Therefore, these could be the reasons for the exception for IPN and BpON.

Based on the calculated k_T values, the lifetime of the studied eight organic nitrates against hydrolysis was calculated at three selected pH values, 3.8, 2.3, and 0.9, corresponding to typical pH values of ambient aerosol particles in Inland regions, China[52–56], Coastal regions, China[57], and Southeastern United States[58], respectively, which are presented in Table 1. It can be found that 3M2BN, TBN, ISO-ON1, ISO-ON2, and BpON have a very short lifetime (in mere minutes or less) and IPN has a lifetime of less than 2.5 h under all three scenarios. Therefore, we concluded that these six organic nitrates can effectively hydrolyze during the lifetime of aerosol particles, which is ~2 weeks[59]. The lifetime of IBN varies from 7 days to 4805 days in three scenarios, indicating that the transformation of IBN is highly dependent on local environmental conditions. However, ETN has a remarkably long lifetime, exceeding 416 days, suggesting that its transformation due to hydrolysis is negligible in the lifecycle of aerosol particles.

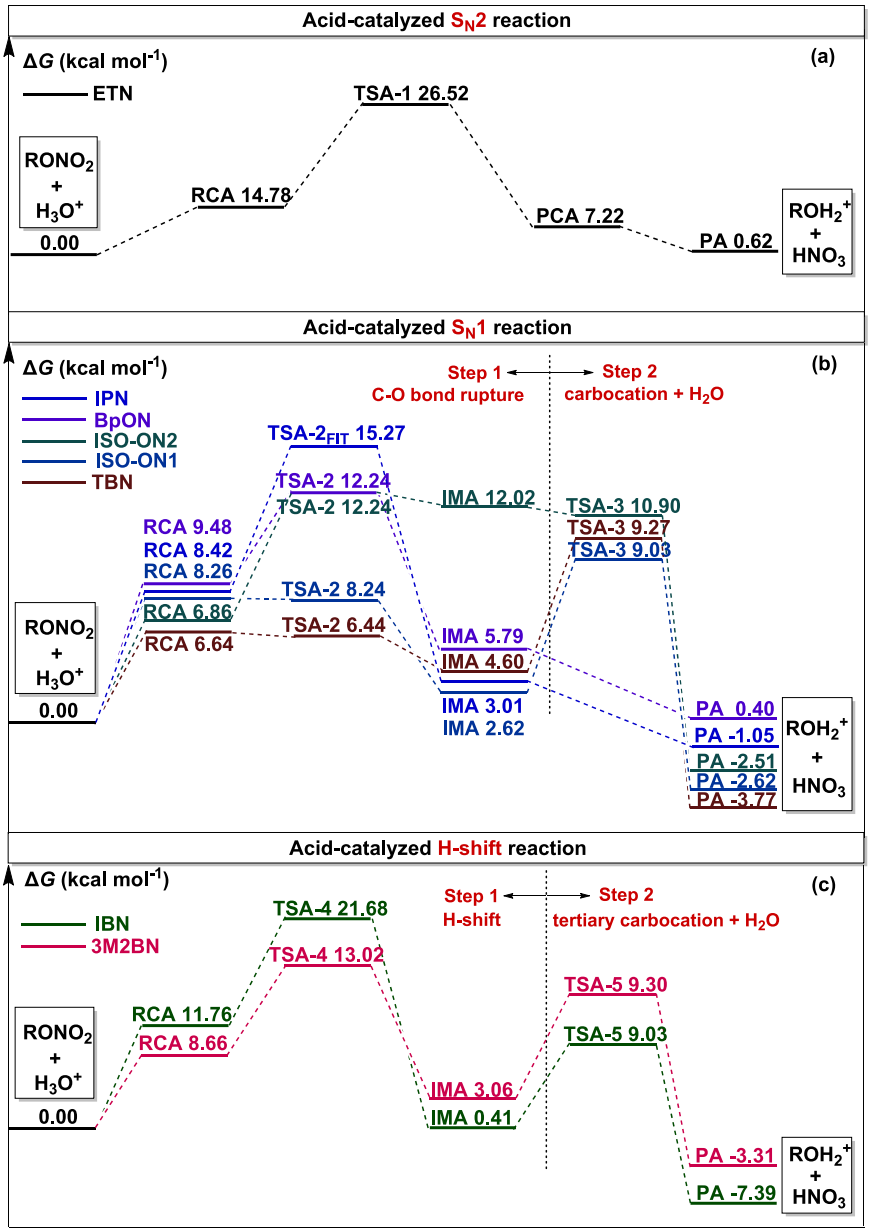

Fig. 7 Calculated schematic free-energy surfaces for the most favorable acid-catalyzed hydrolysis pathway of the studied organic nitrates ($RONO_2$) at the PCM_UFF/CBS-QB3//M06-2X/6-31+G(d,p) level. a Acid-catalyzed S_N2 reaction. **b** Acid-catalyzed S_N1 reaction. **c** Acid-catalyzed H-shift reaction. The free energies of $RONO_2 + H_3O^+$ are set to zero (reference state). RCA, TSA-*m* ($m = 1, 2, 3, 4, 5$), PCA, IMA, and PA represent pre-reactive complexes, transition states, post-reactive complexes, intermediates, and products, where *m* denotes different transition states. $TSA\text{-}2_{FIT}$ denotes the fitted transition state using the relaxed scan method for the S_N1 pathway of IPN.

Structural factors affecting the acid-catalyzed hydrolysis

As discussed above, the acid-catalyzed hydrolysis mechanism is the dominant one for the most considered organic nitrates under typical pH condition in ambient aerosol particles. This is consistent with shorter hydrolysis lifetime of organic nitrates observed at lower pH levels[32,33,39]. Here, we further explored potential structural factors that influence the acid-catalyzed hydrolysis chemistry. By comparing the hydrolysis rates of simple primary, secondary and tertiary organic nitrates (ETN, IPN, and TBN) without additional group, we found that tertiary organic nitrates have the fastest hydrolysis rate, followed by secondary and primary organic nitrates. In addition, other tertiary organic nitrates also exhibited very fast hydrolysis rates, consistent with previous findings[31,34,36]. Therefore, a quaternary C at the α-site is an important structural factor for fast hydrolysis kinetics. Moreover, we found that the hydrolysis rates of primary and secondary organic nitrates containing tertiary C and –C=C at the β-site of the $-ONO_2$ group were significantly faster than those of corresponding primary and secondary organic nitrates without the additional functional groups. The introduction of these functional groups can even make hydrolysis kinetic of primary and secondary organic nitrates (e.g., 3M2BN and BpON) comparable to tertiary organic nitrates. Thus, a tertiary C and –C=C at the β-site of the $-ONO_2$ group is another structural factor for fast hydrolysis kinetics. Combined with the discussion in the hydrolysis kinetics section, the formation of stable carbocation is the intrinsic reason for these three structural factors including the quaternary C at the α-site, tertiary C and –C=C at the β-site of the $-ONO_2$ group. Such a key role of the tertiary C and –C=C at the β-site of the $-ONO_2$ group

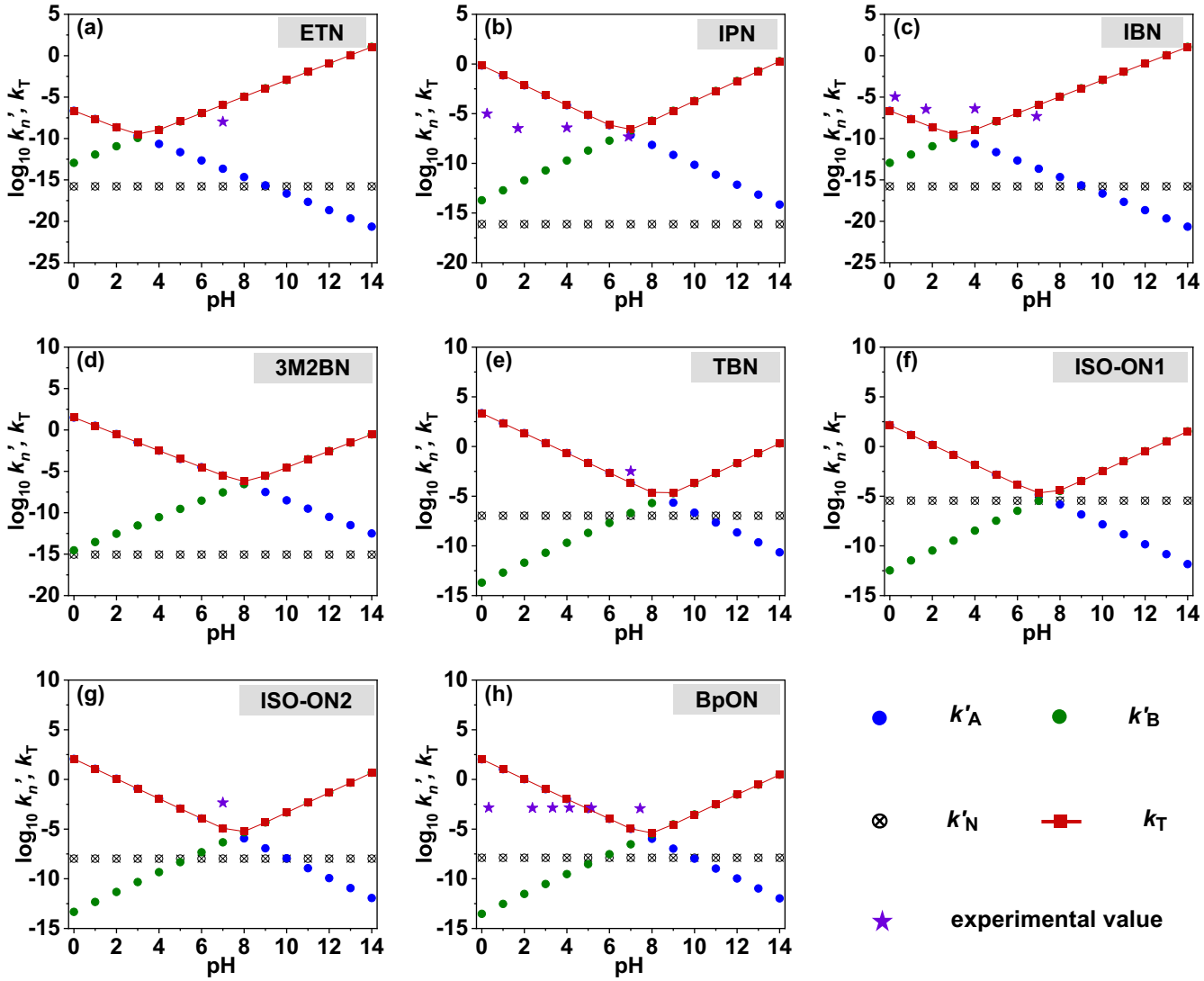

Fig. 8 Logarithmic values of pseudo-first-order hydrolysis rate constant ($\log_{10} k'_{n\ (n\ =\ A,\ B,\ N)}$ and $\log_{10} k_T$) as a function of pH values for eight organic nitrates. a ETN, **b** IPN, **c** IBN, **d** 3M2BN, **e** TBN, **f** ISO-ON1, **g** ISO-ON2 and **h** BpON. k'_A, k'_B, k'_N and k_T indicate acid-catalyzed, basic, neutral and total pseudo-first-order hydrolysis rate constants.

for fast hydrolysis kinetics proposed here is also supported by the previous experimental studies, i.e., IBN and BpON indeed have faster hydrolysis kinetics than simple primary organic nitrates without additional functional groups[35,37].

It is interesting to investigate the possible extrapolation of the revealed important structural factors i.e., tertiary C or –C=C at the β-site of the $-ONO_2$ group. The possible extrapolation of the position of tertiary C or –C=C, from the β-site to the δ-site, and the types of C_β, from tertiary C to quaternary C, were considered. Our results demonstrated that once the position of the tertiary C was changed from the β-site to the γ-site and the δ-site or the position of –C=C from the β-site to the δ-site of the $-ONO_2$ group, the tertiary C and –C=C features no longer played a facilitating role in the hydrolysis of organic nitrates. However, when the position of –C=C was changed from the β-site to the γ-site of the $-ONO_2$ group, it still exhibits a facilitating role while through a cyclization reaction pathway (Supplementary Figs. 34–36). In addition, the quaternary C at the β-site of the $-ONO_2$ group was also found to facilitate the hydrolysis via a two-step reaction pathway initiated by the shift of the methyl cation (Supplementary Figs. 37–40). Therefore, our findings suggest that the facilitating role of tertiary C at the β-site of the $-ONO_2$ group in hydrolysis can be extended to quaternary C, and the position of –C=C can be extrapolated from the β-site to the γ-site of the $-ONO_2$ group. More information about the analysis of structural factors can be seen in Supplementary Discussion.

Computational uncertainties analysis

It is known that a 1 kcal mol^{-1} difference in the activation free energy for an elementary reaction step can lead to one order difference in the calculated reaction rate constants. Therefore, the kinetic calculations are extremely sensitive to the reaction free-energy surface. For the study on the reactions in the aqueous phase, the accuracy of reaction free-energy surface highly depends on the selection of quantum chemical method and solvent model. For the target reactions studied here, the calculated k_T values are consistent with available experimental values at an acceptable level except IPN and BpON at low pH values. Therefore, the selected quantum chemical method and solvent model can be well employed to study target reactions. The recent studies also found the explicit waters have slight effect on

Table 1. Hydrolysis lifetime (τ) of the eight studied organic nitrates in three selected scenarios (Inland regions, China (pH = 3.8); Coastal regions, China (pH = 2.3); Southeastern United States (pH = 0.9)).

Compounds	Inland regions, China	Coastal regions, China	Southeastern United States
ETN	15,206 days	10,230 days	416 days
IBN	4805 days	169 days	7 days
IPN	2.5 h	5 min	11 s
3M2BN	3 min	6 s	<1 s
TBN	3 s	<1 s	<1 s
ISO-ON1	44 s	1 s	<1 s
ISO-ON2	54 s	2 s	<1 s
BpON	59 s	2 s	<1 s

the basic hydrolysis of phthalate esters and parabens when the appropriate quantum chemical method and implicit solvent model were selected[60,61]. If reaction free-energy surface was recalculated at a high level of theory such as CCSD(T) and explicit waters accounting for the solvent effect, which would likely improve the agreement with experiments. However, such high level calculations greatly exceed our computational capabilities at present. More importantly, it is expected that the intrinsic mechanism revealed here cannot be changed even when such calculations were performed in future.

Implications

Our findings in this study have identified important structural factors that facilitate the hydrolysis of organic nitrates, including a quaternary C at the α-site, tertiary C or quaternary C at the β-site of the $-ONO_2$ group and –C=C at β-site or γ-site of the $-ONO_2$ group. These findings provide useful guidelines for assessing the feasibility of hydrolysis for other organic nitrates and serve as a foundation for developing fragmentation-based predictive models for the hydrolysis kinetics. However, it is worth noting that organic nitrates present in ambient aerosol particles could contain other functional groups, such as –OH, –OOH and –C=O[21,43,62], which can also affect hydrolysis chemistry. Our preliminary study found that tertiary organic nitrates with –OH and –OOH at the β-site of $-ONO_2$ group still exhibit fast kinetics, although the introduction of –OH and –OOH decreases the hydrolysis rate to a certain extent (less than two orders of magnitude). However, introducing a –C=O at the β-site of the $-ONO_2$ group significantly decreases the hydrolysis rate (up to nine orders of magnitude), making the significance of hydrolysis highly depend on the pH of the aerosol during the lifecycle of aerosol particles (Supplementary Figs. 41–43 and Supplementary Table 2). Therefore, further research is warranted to investigate the impact of multiple functional groups on hydrolysis chemistry to clearly understand the hydrolysis of multi-functional organic nitrates.

This study has revealed that the formation of stable carbocations is a common feature for the fast hydrolysis of organic nitrates. It should be noted that there is a plethora of other organics in ambient aerosol particles. Recent studies found that the carbocations from methylglyoxal and glyoxal can react with other compounds such as diols/tetrol and ammonia to produce oligomers and N-heterocycles[63–65], changing the composition and properties of aerosol particles. Thus, it is highly possible that the formed carbocations in the hydrolysis of organic nitrates also interact with other compounds to form oligomers and N-heterocycles. Therefore, further research is necessary to explore the impact of hydrolysis chemistry of the organic nitrates on the component and properties of aerosol particles.

METHODS

Electronic structure calculations

All the structure optimizations and energy calculations were performed within the Gaussian 09 program package[66]. The geometry optimization and frequency calculation of the reactants (R), products (P), TS, pre-reactive complexes (RC), post-reactive complexes (PC) and intermediates (IM) were carried out at the M06-2X/6-31 + G(d,p) level of theory[67]. Intrinsic Reaction Coordinate (IRC) calculations were implemented to confirm that each TSs connect the specified reactants and products at the same theoretical level as that of corresponding geometry optimization[68]. For the reaction pathways we cannot successfully locate the TSs, the free-energy surfaces were fitted using relaxed scan method, which is described in detail in Supplementary Methods. Single-point energy (SPE) calculations of all species were performed at a higher-level calculation using the CBS-QB3 method[69]. The polarizable continuum model (PCM) with the universal force field (UFF) radii was applied by comparing with the solvation model based on density (SMD) for the geometry optimization, frequency and SPE calculation (Supplementary Tables 3 and 4)[70,71]. For simplicity, the employed methods are denoted as the W/X//Y, i.e., PCM_UFF/CBS-QB3//M06-2X/6-31 + G(d,p) level. The Gibbs free energy (G) values at 298.15 K for each species were obtained by combining SPE and Gibbs correction energy calculated at the theoretical level of geometry optimization. Activation free energy ($\Delta G^{\ddagger}$) and reaction free energy ($\Delta_r G$) were obtained by calculating the G difference between R and corresponding TS, and R and P, respectively. A correction factor of 1.89 kcal mol^{-1} was applied in the calculation of $\Delta G^{\ddagger}$ and $\Delta_r G$ values for reactions where the molecular number decreases or increases by one from R to TS or from R to P to explain the free energy change from the gas phase standard state of 1 atm to the aqueous phase standard state of 1 mol L^{-1} [72]. In addition, global minimum was chosen as the starting configuration of reactants to study the target reactions. Details for global minimum search were provided in Supplementary Methods.

Reaction rate constant calculation

The second-order reaction rate constant (k) of the elementary reactions was calculated by the transition state theory[61,73,74]:

$$k = \kappa (c^{\circ})^{\triangle n} \frac{k_b}{h} \exp\left(-\frac{\Delta G^{\ddagger}}{RT}\right) \quad (1)$$

where c° is the standard-state concentration (1 mol L^{-1}), Δn is the change in the number of moles from R to TS, T is the temperature (298.15 K), k_b is Boltzmann constant (J K^{-1}), h is the Planck constant (J s), R is the gas constant (8.314 J mol^{-1} K^{-1}), $\Delta G^{\ddagger}$ is activation free energy.

κ is the Winger transmission coefficient, which is 1 for all reactions except H-abstraction and H-shift reaction. κ can be calculated by Eq. 2 for H-abstraction and H-shift reaction[75,76].

$$\kappa = 1 + \frac{1}{24}\left(\frac{h\nu_i^{\ddagger}}{k_b T}\right)^2 \quad (2)$$

For the two and three step reaction pathways, the pseudo-first-order rate constants were calculated by applying steady-state approximations and the transition state theory (Supplementary Eqs. 4, 7, 11 and 14)[74]. By taking into account the neutral, basic, and acid-catalyzed reactions, the total pseudo-first-order rate constants (k_T) can be calculated by Eq. 3[75], and the lifetime (τ) of organic nitrates caused by the hydrolysis is expressed as the reciprocal of k_T.

$$k_T = k'_N + k'_B + k'_A \quad (3)$$

where k'_N, k'_B, and k'_A (s^{-1}) are the neutral, basic and acid-catalyzed pseudo-first-order hydrolysis rates, respectively. Exactly,

for the unimolecular pathway, the k'_N, k'_B, and k'_A (s^{-1}) are the reaction rate constants calculated by the transition state theory; for the bimolecular reaction pathway, the pseudo-first-order rate constants were employed by considering the concentration of another reacting partner.

DATA AVAILABILITY

All data were available in the main text or supplementary information. The other relevant data are available upon request from the corresponding authors.

Received: 19 January 2023; Accepted: 2 November 2023;
Published online: 18 November 2023

REFERENCES

1. De Gouw, J. & Jimenez, J. L. Organic aerosols in the earth's atmosphere. *Environ. Sci. Technol.* **43**, 7614–7618 (2009).
2. Zhou, W. et al. A review of aerosol chemistry in Asia: insights from aerosol mass spectrometer measurements. *Environ. Sci. Process. Impacts* **22**, 1616–1653 (2020).
3. McNeill, V. F. Aqueous organic chemistry in the atmosphere: sources and chemical processing of organic aerosols. *Environ. Sci. Technol.* **49**, 1237–1244 (2015).
4. Schone, L. et al. Atmospheric aqueous phase radical chemistry of the isoprene oxidation products methacrolein, methyl vinyl ketone, methacrylic acid and acrylic acid-kinetics and product studies. *Phys. Chem. Chem. Phys.* **16**, 6257–6272 (2014).
5. Pospisilova, V. et al. On the fate of oxygenated organic molecules in atmospheric aerosol particles. *Sci. Adv.* **6**, No. eaax8922 (2020).
6. Tilgner, A. et al. Acidity and the multiphase chemistry of atmospheric aqueous particles and clouds. *Atmos. Chem. Phys.* **21**, 13483–13536 (2021).
7. Otto, T., Stieger, B., Mettke, P. & Herrmann, H. Tropospheric aqueous-phase oxidation of isoprene-derived dihydroxycarbonyl compounds. *J. Phys. Chem. A* **121**, 6460–6470 (2017).
8. Zhang, Y. Q. et al. Observational insights into isoprene secondary organic aerosol formation through the epoxide pathway at three urban sites from northern to southern China. *Environ. Sci. Technol.* **56**, 4795–4805 (2022).
9. Zheng, Y. et al. Precursors and pathways leading to enhanced secondary organic aerosol formation during severe haze episodes. *Environ. Sci. Technol.* **55**, 15680–15693 (2021).
10. Abellar, K. A., Cope, J. D. & Nguyen, T. B. Second-order kinetic rate coefficients for the aqueous-phase hydroxyl radical (·OH) oxidation of isoprene-derived secondary organic aerosol compounds at 298 K. *Environ. Sci. Technol.* **55**, 13728–13736 (2021).
11. McNeill, V. F. et al. Aqueous-phase secondary organic aerosol and organosulfate formation in atmospheric aerosols: a modeling study. *Environ. Sci. Technol.* **46**, 8075–8081 (2012).
12. Li, Y. et al. Unexpected oligomerization of small α-dicarbonyls for secondary organic aerosol and brown carbon formation. *Environ. Sci. Technol.* **55**, 4430–4439 (2021).
13. Zare, A., Fahey, K. M., Sarwar, G., Cohen, R. C. & Pye, H. O. T. Vapor-pressure pathways initiate but hydrolysis products dominate the aerosol estimated from organic nitrates. *ACS Earth Space Chem.* **3**, 1426–1437 (2019).
14. Ng, N. L. et al. Nitrate radicals and biogenic volatile organic compounds: oxidation, mechanisms, and organic aerosol. *Atmos. Chem. Phys.* **17**, 2103–2162 (2017).
15. Lin, C., Huang, R.-J., Duan, J., Zhong, H. & Xu, W. Primary and secondary organic nitrate in northwest China: a case study. *Environ. Sci. Technol. Lett.* **8**, 947–953 (2021).
16. Kiendler-Scharr, A. et al. Ubiquity of organic nitrates from nighttime chemistry in the European submicron aerosol. *Geophys. Res. Lett.* **43**, 7735–7744 (2016).
17. Yu, K., Zhu, Q., Du, K. & Huang, X.-F. Characterization of nighttime formation of particulate organic nitrates based on high-resolution aerosol mass spectrometry in an urban atmosphere in China. *Atmos. Chem. Phys.* **19**, 5235–5249 (2019).
18. Berkemeier, T., Ammann, M., Mentel, T. F., Poschl, U. & Shiraiwa, M. Organic nitrate contribution to new particle formation and growth in secondary organic aerosols from α-pinene ozonolysis. *Environ. Sci. Technol.* **50**, 6334–6342 (2016).
19. Xu, L., Suresh, S., Guo, H., Weber, R. J. & Ng, N. L. Aerosol characterization over the southeastern United States using high-resolution aerosol mass spectrometry: spatial and seasonal variation of aerosol composition and sources with a focus on organic nitrates. *Atmos. Chem. Phys.* **15**, 7307–7336 (2015).
20. Kenagy, H. S. et al. Contribution of organic nitrates to organic aerosol over South Korea during KORUS-AQ. *Environ. Sci. Technol.* **55**, 16326–16338 (2021).
21. Lee, B. H. et al. Highly functionalized organic nitrates in the southeast United States: contribution to secondary organic aerosol and reactive nitrogen budgets. *Proc. Natl Acad. Sci. USA* **113**, 1516–1521 (2016).
22. Shi, X. et al. Isomeric identification of particle-phase organic nitrates through gas chromatography and time-of-flight mass spectrometry coupled with an electron capture negative ionization source. *Environ. Sci. Technol.* **54**, 707–713 (2020).
23. Perring, A. E., Pusede, S. E. & Cohen, R. C. An observational perspective on the atmospheric impacts of alkyl and multifunctional nitrates on ozone and secondary organic aerosol. *Chem. Rev.* **113**, 5848–5870 (2013).
24. Chen, X., Wang, H. & Lu, K. Simulation of organic nitrates in Pearl River Delta in 2006 and the chemical impact on ozone production. *Sci. China Earth Sci.* **61**, 228–238 (2018).
25. Fisher, J. A. et al. Organic nitrate chemistry and its implications for nitrogen budgets in an isoprene- and monoterpene-rich atmosphere: constraints from aircraft (SEAC^{4}RS) and ground-based (SOAS) observations in the Southeast US. *Atmos. Chem. Phys.* **16**, 5969–5991 (2016).
26. Browne, E. C. et al. Observations of total $RONO_2$ over the boreal forest: NO*x* sinks and HNO_3 sources. *Atmos. Chem. Phys.* **13**, 4543–4562 (2013).
27. Zare, A. et al. A comprehensive organic nitrate chemistry: insights into the lifetime of atmospheric organic nitrates. *Atmos. Chem. Phys.* **18**, 15419–15436 (2018).
28. Liu, S. et al. Hydrolysis of organonitrate functional groups in aerosol particles. *Aerosol Sci. Technol.* **46**, 1359–1369 (2012).
29. Takeuchi, M. & Ng, N. L. Chemical composition and hydrolysis of organic nitrate aerosol formed from hydroxyl and nitrate radical oxidation of α-pinene and β-pinene. *Atmos. Chem. Phys.* **19**, 12749–12766 (2019).
30. Bean, J. K. & Hildebrandt Ruiz, L. Gas-particle partitioning and hydrolysis of organic nitrates formed from the oxidation of α-pinene in environmental chamber experiments. *Atmos. Chem. Phys.* **16**, 2175–2184 (2016).
31. Vasquez, K. T. et al. Rapid hydrolysis of tertiary isoprene nitrate efficiently removes NO*x* from the atmosphere. *Proc. Natl Acad. Sci. USA* **117**, 33011–33016 (2020).
32. Hu, K. S., Darer, A. I. & Elrod, M. J. Thermodynamics and kinetics of the hydrolysis of atmospherically relevant organonitrates and organosulfates. *Atmos. Chem. Phys.* **11**, 8307–8320 (2011).
33. Morales, A. C., Jayarathne, T., Slade, J. H., Laskin, A. & Shepson, P. B. The production and hydrolysis of organic nitrates from OH radical oxidation of β-ocimene. *Atmos. Chem. Phys.* **21**, 129–145 (2021).
34. Darer, A. I., Cole-Filipiak, N. C., O'Connor, A. E. & Elrod, M. J. Formation and stability of atmospherically relevant isoprene-derived organosulfates and organonitrates. *Environ. Sci. Technol.* **45**, 1895–1902 (2011).
35. Wang, Y. et al. Synthesis and hydrolysis of atmospherically relevant monoterpene-derived organic nitrates. *Environ. Sci. Technol.* **55**, 14595–14606 (2021).
36. Vesto, J. I. et al. Condensed phase kinetic studies of hydroxynitrates derived from the photooxidation of carene, limonene, trans-carveol, and perillic alcohol. *Atmosphere* **13**, 592 (2022).
37. Rindelaub, J. D. et al. The acid-catalyzed hydrolysis of an α-pinene-derived organic nitrate: kinetics, products, reaction mechanisms, and atmospheric impact. *Atmos. Chem. Phys.* **16**, 15425–15432 (2016).
38. Keshavarz, F., Thornton, J. A., Vehkamäki, H. & Kurtén, T. Reaction mechanisms underlying unfunctionalized alkyl nitrate hydrolysis in aqueous aerosols. *ACS Earth Space Chem.* **5**, 210–225 (2021).
39. Rindelaub, J. D., McAvey, K. M. & Shepson, P. B. The photochemical production of organic nitrates from α-pinene and loss via acid-dependent particle phase hydrolysis. *Atmos. Environ.* **100**, 193–201 (2015).
40. Jacobs, M. I., Burke, W. J. & Elrod, M. J. Kinetics of the reactions of isoprene-derived hydroxynitrates: gas phase epoxide formation and solution phase hydrolysis. *Atmos. Chem. Phys.* **14**, 8933–8946 (2014).
41. Pye, H. O. et al. Modeling the current and future roles of particulate organic nitrates in the southeastern United States. *Environ. Sci. Technol.* **49**, 14195–14203 (2015).
42. Romer Present, P. S., Zare, A. & Cohen, R. C. The changing role of organic nitrates in the removal and transport of NO*x*. *Atmos. Chem. Phys.* **20**, 267–279 (2020).
43. Huang, W. et al. Chemical characterization of highly functionalized organonitrates contributing to night-time organic aerosol mass loadings and particle growth. *Environ. Sci. Technol.* **53**, 1165–1174 (2019).
44. Zhang, Y. et al. Observations of C_1-C_5 alkyl nitrates in the Yellow River Delta, northern China: effects of biomass burning and oil field emissions. *Sci. Total. Environ.* **656**, 129–139 (2019).
45. Zeng, L., Lyu, X., Guo, H., Zou, S. & Ling, Z. Photochemical formation of C_1-C_5 alkyl nitrates in suburban Hong Kong and over the south China Sea. *Environ. Sci. Technol.* **52**, 5581–5589 (2018).
46. Sun, J. et al. Summertime C_1-C_5 alkyl nitrates over Beijing, northern China: spatial distribution, regional transport, and formation mechanisms. *Atmos. Res.* **204**, 102–109 (2018).

47. Ryu, H. et al. Pitfalls in computational modeling of chemical reactions and how to avoid them. *Organometallics* **37**, 3228–3239 (2018).
48. Olah, G. A. 100 years of carbocations and their significance in chemistry. *J. Org. Chem.* **66**, 5943–5957 (2001).
49. Alamiddine, Z. & Humbel, S. Hyperconjugation in carbocations, a BLW Study with DFT approximation. *Front. Chem.* **1**, 37 (2014).
50. Naredla, R. R. & Klumpp, D. A. Contemporary carbocation chemistry: applications in organic synthesis. *Chem. Rev.* **113**, 6905–6948 (2013).
51. Pye, H. O. T. et al. The acidity of atmospheric particles and clouds. *Atmos. Chem. Phys.* **20**, 4809–4888 (2020).
52. Ding, J. et al. Aerosol pH and its driving factors in Beijing. *Atmos. Chem. Phys.* **19**, 7939–7954 (2019).
53. Shi, X. et al. High-resolution data sets unravel the effects of sources and meteorological conditions on nitrate and its gas-particle partitioning. *Environ. Sci. Technol.* **53**, 3048–3057 (2019).
54. Wang, S. et al. Effect of ammonia on fine-particle pH in agricultural regions of China: comparison between urban and rural sites. *Atmos. Chem. Phys.* **20**, 2719–2734 (2020).
55. Xu, J. et al. Importance of gas-particle partitioning of ammonia in haze formation in the rural agricultural environment. *Atmos. Chem. Phys.* **20**, 7259–7269 (2020).
56. Jia, S. et al. Technical note: comparison and interconversion of pH based on different standard states for aerosol acidity characterization. *Atmos. Chem. Phys.* **18**, 11125–11133 (2018).
57. Wang, G. et al. Quantitative decomposition of influencing factors to aerosol pH variation over the coasts of the South China Sea, East China Sea, and Bohai Sea. *Environ. Sci. Technol. Lett.* **9**, 815–821 (2022).
58. Guo, H. et al. Fine-particle water and pH in the southeastern United States. *Atmos. Chem. Phys.* **15**, 5211–5228 (2015).
59. Kristiansen, N. I. et al. Evaluation of observed and modelled aerosol lifetimes using radioactive tracers of opportunity and an ensemble of 19 global models. *Atmos. Chem. Phys.* **16**, 3525–3561 (2016).
60. Xu, T. et al. Prediction models on pKa and base-catalyzed hydrolysis kinetics of parabens: experimental and quantum chemical studies. *Environ. Sci. Technol.* **55**, 6022–6031 (2021).
61. Xu, T. et al. Development of prediction models on base-catalyzed hydrolysis kinetics of phthalate esters with density functional theory calculation. *Environ. Sci. Technol.* **53**, 5828–5837 (2019).
62. DeVault, M. P., Ziola, A. C. & Ziemann, P. J. Products and mechanisms of secondary organic aerosol formation from the NO_3 radical-initiated oxidation of cyclic and acyclic monoterpenes. *ACS Earth Space Chem.* **6**, 2076–2092 (2022).
63. Ji, Y. et al. Elucidating the critical oligomeric steps in secondary organic aerosol and brown carbon formation. *Atmos. Chem. Phys.* **22**, 7259–7271 (2022).
64. Ji, Y. et al. Carbenium ion-mediated oligomerization of methylglyoxal for secondary organic aerosol formation. *Proc. Natl Acad. Sci. USA* **117**, 13294–13299 (2020).
65. Zhang, Y., He, L., Sun, X., Ventura, O. N. & Herrmann, H. Theoretical investigation on the oligomerization of methylglyoxal and glyoxal in aqueous atmospheric aerosol particles. *ACS Earth Space Chem.* **6**, 1031–1043 (2022).
66. Frisch, M. J. et al. Gaussian 09 revision A.1 (2009).
67. Zhao, Y. & Truhlar, D. G. The M06 suite of density functionals for main group thermochemistry, thermochemical kinetics, noncovalent interactions, excited states, and transition elements: two new functionals and systematic testing of four M06-class functionals and 12 other functionals. *Theor. Chem. Acc.* **120**, 215–241 (2008).
68. Fukui, K. The path of chemical reactions—the IRC approach. *Acc. Chem. Res.* **14**, 363–368 (1981).
69. Montgomery, J. A., Frisch, M. J., Ochterski, J. W. & Petersson, G. A. A complete basis set model chemistry. VI. Use of density functional geometries and frequencies. *J. Chem. Phys.* **110**, 2822–2827 (1999).
70. Tomasi, J., Mennucci, B. & Cammi, R. Quantum mechanical continuum solvation models. *Chem. Rev.* **105**, 2999–3094 (2005).
71. Rappe, A. K., Casewit, C. J., Colwell, K. S., Goddard, W. A. & Skiff, W. M. UFF, a full periodic table force field for molecular mechanics and molecular dynamics simulations. *J. Am. Chem. Soc.* **114**, 10024–10035 (1992).
72. Sadlej-Sosnowska, N. Calculation of acidic dissociation constants in water: solvation free energy terms. Their accuracy and impact. *Theor. Chem. Acc.* **118**, 281–293 (2007).
73. Yu, Q. et al. Computational investigation of the nitrosation mechanism of piperazine in CO_2 capture. *Chemosphere* **186**, 341–349 (2017).
74. Galano, A. & Alvarez-Idaboy, J. R. Guanosine + OH radical reaction in aqueous solution: a reinterpretation of the UV-vis data based on thermodynamic and kinetic calculations. *Org. Lett.* **11**, 5114–5117 (2009).
75. Zhang, H., Xie, H., Chen, J. & Zhang, S. Prediction of hydrolysis pathways and kinetics for antibiotics under environmental pH conditions: a quantum chemical study on cephradine. *Environ. Sci. Technol.* **49**, 1552–1558 (2015).
76. Louis, F., Gonzalez, C. A., Huie, R. E. & Kurylo, M. J. An ab initio study of the kinetics of the reactions of halomethanes with the hydroxyl radical. 1. CH_2Br_2. *J. Phys. Chem. A* **104**, 2931–2938 (2000).

ACKNOWLEDGEMENTS

This study was supported by the National Natural Science Foundation of China (22236004, 22206020, 22176022), the China Postdoctoral Science Foundation (2022M720640), the National Key Research and Development Program of China (2022YFC3701000, Task1).

AUTHOR CONTRIBUTIONS

H.X. contributed to conceiving the idea, analyzing results, editing, and revision. Q.Z. contributed to performing DFT calculations, analyzing results, interpreting data, and writing the original draft. F.M., W.N., C.Y., D.H., J.E., and J.C. contributed to editing and revision. All authors read and approved the final manuscript.

COMPETING INTERESTS

The authors declare no competing interests.

ADDITIONAL INFORMATION

Supplementary information The online version contains supplementary material available at https://doi.org/10.1038/s41612-023-00517-w.

Correspondence and requests for materials should be addressed to Hong-Bin Xie.

Reprints and permission information is available at http://www.nature.com/reprints

Publisher's note Springer Nature remains neutral with regard to jurisdictional claims in published maps and institutional affiliations.